Unifying the Oxygen Reduction and Evolution Reaction with Surface Oxygen and Extracting their Intrinsic Activities on Platinum Catalysts

Supplemental Information

Benedikt A Brandes, Yogeshwaran Krishnan, Fabian L Buchauer, Heine A Hansen, and Johan Hjelm

1. Electrochemistry

All measurements were performed in a three-electrode glass cell with an electrolyte volume of about 40 ml. The counter and reference electrode were each placed in a compartment separated by a glass frit to the working electrode. As reference electrode served a platinum wire submersed in an atmosphere of electrolytically produced hydrogen and electrolyte. A platinum wire served as counter electrode. We used a home-made glass cell filled with either 0.1 M $HClO_4$ or a 0.1 M H_2SO_4 solution as the electrolytes and a Pine R(R)DE rotator together with a Biologic potentiostat for all measurements.

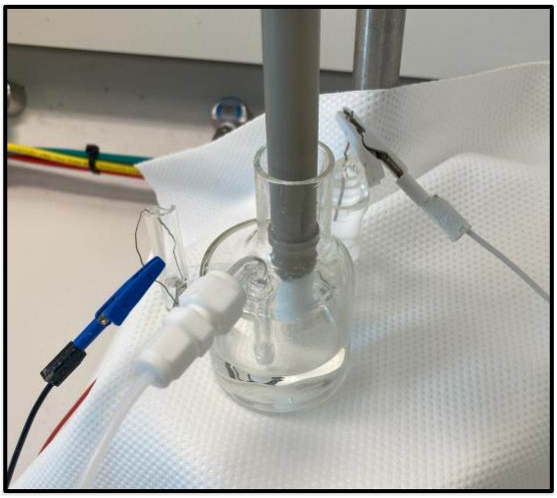

Fig. S1a| Electrochemical cell and measurement setup. The reference electrode can be removed to be filled with electrolyte. The counter and reference electrode compartments are separated from the main compartment by glass frits (lower porosity for the counter electrode compartment than for the reference electrode compartment). The liquid volume of the cell is about 50 ml and reaches gas saturation very fast thanks to the frit on the bubbler. An extra hose to blanket the cell rather than bubble the gas was used in sensitive experiments, such as SPEIS.

Electrolytes

In this work only one kind of stock solution of each perchloric acid ($HClO_4$), sulfuric acid (H_2SO_4) and hydrochloric acid (HCl) was used. We used Perchloric acid, TraceSelect (65-71%) from Honeywell/Fluka, catalogue number 77227-500ML, batch number J0940. Still, obtaining sufficiently pure perchloric acid remains to be a gamble. As sulfuric acid we used analytical grade sulfuric acid ≥95% from Fisher Scientific (S/9240/PB15, batch number 2231877). Fuming hydrochloric acid was obtained from Sigma-Aldrich (Merck KgA). The stock solutions were then diluted with 18.2 MΩ deionized water to approximately 0.1

molarity. The electrolyte was frequently changed during the measurement series, certainly before conducting any ORR measurements.

Gases

All gases were supplied by building gas lines (DTU Lyngby Campus, building 310). Professionally installed and monitored about 3 years before this study. The argon and oxygen are sourced by evaporation from a liquid source (5N) resulting in a quality close to 6N. The hydrogen (3.5N) and CO (3.0N) supplies were the greatest concern regarding impurities and no critical measurements were performed after these gases were used without changing the electrolyte.

Electrodes

Two kinds of electrodes served as working electrode (5 mm diameter): A fixed Pt crystal electrode and an exchangeable electrode with a separate Pt_xCo- and Pt_xNi-crystal insert (4 mm height). The latter were obtained from Mateck GmbH, Germany with a nominal Pt:M ratio of 3:1. The platinum electrode was polished frequently but not prior every experiment. The Pt alloy surfaces were polished every time before use. It was sufficient to polish the electrodes briefly only with a 0.3 µm alumina suspension on a nap cloth to obtain a defect free mirror like finish. For the Pt/C measurements we drop-casted 10 µl of a horn sonication assisted dispersion of Ketjenblack supported Pt nanoparticles (40% Pt loading, Fuel Cell Store, Batch 100383-4004) in ethanol (0.49 $ml_{Ethanol}/mg_{Catalyst}$, 1.3 $µl/mg_{Catalyst}$, 5% Nafion solution) on a 5 mm diameter glassy carbon disc, obtaining an electrode loading of 10 $µg_{Pt}/cm^2$ with a theoretical film thickness of 1.57 µm. The roughness factor was determined by the CO displacement technique to be 8-9 cm^2/cm^2 compared to 1.3 cm^2/cm^2 of the Pt(pc) and Pt-alloy(pc) electrodes.

HFR measurement

The high frequency resistance (HFR) was measured by potentiostatic electrochemical impedance spectroscopy (PEIS) at 450 mV from 1kHz to 100 Hz (6 points per decade) with a voltage perturbation of 5 mV. The real part of the impedance of the closest point to the real axis in a Nyquist plot was used as the HFR value. The electrolyte was saturated either by Argon, O2, H2 or any mixture of these gases during a transition between experimental procedures as this does not influence the value of the HFR.

RHE potential measurement

The reversible hydrogen electrode (RHE) potential was measured by bubbling H_2 on the working electrode while the open circuit voltage (OCV) is recorded until a stable potential was obtained. Occasional rotation bursts sped up this process. This value was used to correct all potentials in subsequent or previous measurements that can reasonable associated to this RHE potential so that the RHE potential is zero as per its definition.

Scanning Potential Electrochemical Impedance Spectroscopy (SPEIS) Measurements

The SPEIS measurements were performed between 50 mV and 1200 mV with each measurement point being 25 mV apart. Each measurement consisted of an initial rest time of 1 s and measurement of a single frequency for about 1.5 s with a voltage perturbation of 5 mV and 3.5 mV_{rms} , overall corresponding to a scan rate of 10 mV/s. Only the imaginary part was used to construct the respective CV according to the following equation:

$$C(E,f) = C_{\mathrm{DL}} \frac{\mathrm{Im}(Z(E,f))}{\mathrm{Im}(Z(E_{DL},f))} \tag{S1a}$$

$\mathrm{C_{DL}}$ is the double layer capacitance and $\mathrm{E_{DL}}$ is any potential in the double layer region where $\mathrm{C}(E) = C_{DL}$, Z is the measures impedance at a given frequency. Note that the SPEIS technique with one single frequency per potential value was chosen instead of the equivalent AC voltammetry due to limitation in the EC-Lab software of the Biologic instrument.

Cleanliness of the electrolyte and roughness of the electrode

Only measurements that reach a sufficient level of cleanliness were accepted to be part of this work. Consequently, the criteria were established, that at a scan rate of 50 mV/s in CV between 60 mV and 1200 mV under Argon atmosphere the main positive H-upd peak must reach least 17 µA (67 µA/cm^2) once cycling profile stabilizes. This value was used both for 0.1 M $HClO_4$ and 0.1 H_2SO_4. When the electrode is rotated, the mass transport to the electrode greatly increases, leading to a substantial increase in the amount of trace impurities (or Pt poisons) reaching the Pt surface. Their effect is noted by a more pronounced peak in the negative scan direction around 300 mV and a decrease in the *OH formation around 850 mV and flattening of the electrochemical irreversible O-upd feature. Such a behaviors is consistent with the adsorption of anions, such as sulfate, phosphates, and halogenides. We expect chloride and hypo-chlorides as the main impurity in the perchloric acid used here. We have the conjecture that variations in the impurities of the same perchloric acid, but different batches, stem from the distillation process. Commonly, the purist perchloric acids are targeted towards trace metal analysis where the anions do not play a significant role. Often enough, trace anions are not even quantified which has been often enough a great disappointment when receiving a new batch of the same perchloric acid. Some publications find unsymmetric peak at around 170 mV in the cathodic scan instead of the shoulder at 300 mV. We are very certain that this is a sign of anion interferences and consequently a substandard level of cleanliness of the electrolyte. To maintain cleanliness of the glass cell and all relevant components we utilize frequent and extensive boiling in 18.2 MΩ water. We find this to be the most efficient and safe way compared to e.g., using the infamous piranha bath method. Additionally, any items in contact with the electrochemical cell were only touched with fresh cleanroom gloves and placed on fresh lint-free cleanroom-compatible cloths. The inside of the electrochemical cell was never touched.

When the electrode is not frequently polished, the overall currents will drop. We have seen electrodes changing the roughness factor from 1.3 cm^2/cm^2 to 1.1 cm^2/cm^2 by maintaining the overall characteristic CV. It appears that due to frequent cycling and redeposition during the O-upd reduction, the surface is flattened further and loses surface area while the composition of sites does not change. Therefore, we polished the electrodes prior to any measurement series. The electrochemical active surface area (ECSA) and hence the roughness factor was determined by both H-upd and CO stripping of the electrodes, both at 50 mV/s. Both values agreed within 5% on Pt(pc).

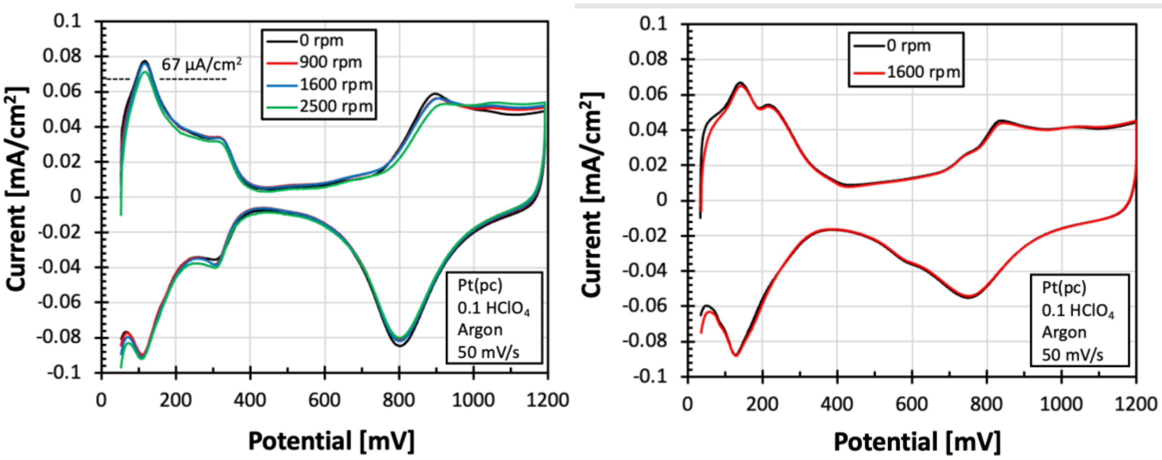

Fig. S1b| Left CVs of Pt(pc) at different rotation rates. **Right** CVs of Pt/C at different rotation rates.

Pseudocapacitive O-upd

Fig. S1c displace the capacitance of the CV on platinum at different scan rates. One can clearly see the effect of the HER at lower scan rates by the shift in the H-upd formation peak. This is due to the superposition in HER and H-upd currents, with the first remaining constant while the latter decreasing at lower scan rates. The higher negative capacitance at lower scan rates appears to originate from more strongly bound oxygen species formed at high potentials in the O-upd region. The shift in the O-upd formation peak in contrast must originate from kinetic limitations. This has been demonstrated on Pt(111) in literature and in our laboratory (not shown) and the peak may be attributed to the Pt(111) features of Pt(pc).

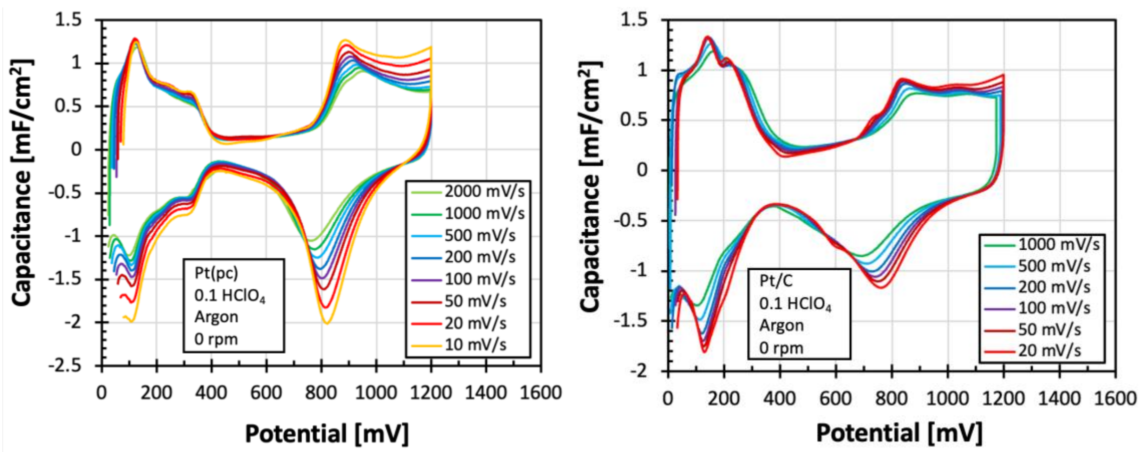

Fig S1c| Left CVs of Pt(pc) at different scan rates. **Right** CVs of Pt/C at different scan rates

Protocol of the ORR kinetic analysis

In case polycrystalline platinum was measured, the protocol demanded that the surface is fully reconstructed and stable. This was achieved by excessively cycling the surface between 50 mV and 1200 mV at high scan rates of 500 mV/s. Once a stable CV way obtained, a 50 mV CV was recorded and compared against the CV in Fig. S1b. Subsequently the HFR and RHE potential were measured. The electrolyte was changed, and the O-upd/oxygen surface charge was measured as described. Another set of HFR and RHE potentials was measured before changing the electrolyte again and now the ORR activity was measured followed by another set of HFR and RHE potentials. In case the reconstruction of polycrystalline platinum or platinum alloys were used as specimen, the upper vertex potential was limited. At first however, the surface is cycled 50 times at 500 mV/s 50 mV above the specified vertex potential. This ensures that the surface will not change further at subsequent measurements that stay under this limit. Then the surface is cycled 50 times at 500 mV/s to the specified upper vertex potential and the original protocol is followed. Minor deviations of the protocol were accepted if they are uncritical.

Measurement of the oxygen charge and ORR activity for the kinetic analysis

The various oxygen charges on the platinum surface were measured by a series of CVs for one specific scan rate in Argon. This protocol consists of two kinds of CVs: (1) A CV that ensures that every CV is obtained from the same surface and the actual CV. This CV consists of 5 cycles between 50 mV and the maximum potential of this measurement series at 500 mV/s. The actual CV consists of 2 cycles between 200 mV and a varied upper vertex potential at the specified scan rate. Finally, the HFR and the RHE was measured, and the electrolyte was changed. The ORR activity was then measured similarly in oxygen and turning on the rotation to 1600 rpm. While the CVs ensuring a consistent surface remain the same, LSVs are chosen instead of CVs (with notable exceptions for the time effect) for the actual measurements.

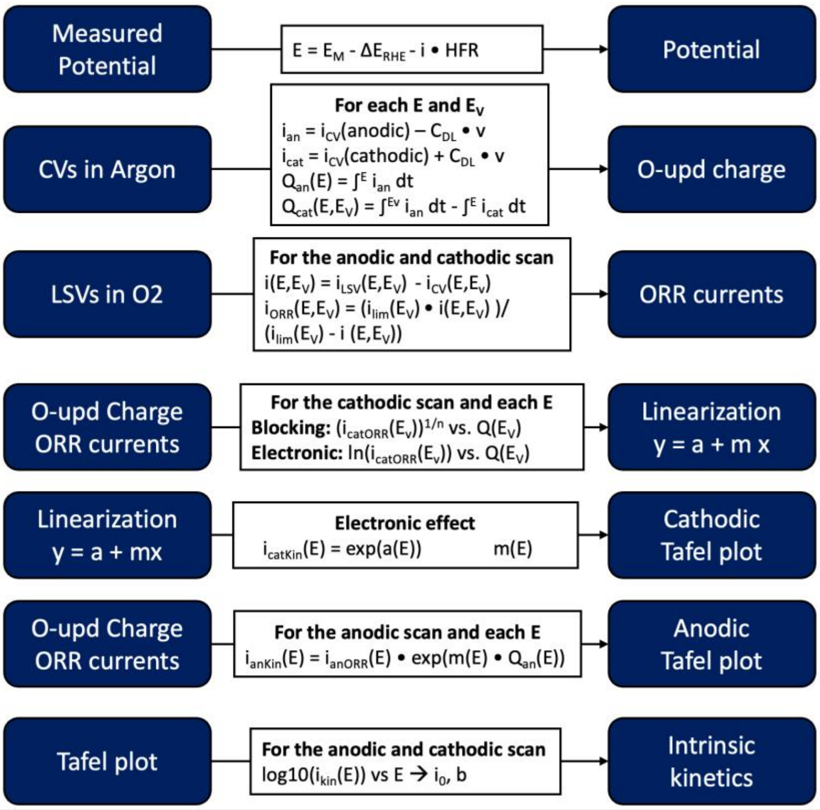

Fig. S1d| Protocol of analyzing the experimental data to obtain the oxide-free ORR kinetics.

The time effect of the O-upd on the ORR

The time effect of the O-upd effect was probed by holding the potential for set times at a potential of 1200 mV. During the holding period, other reactions occur on the electrode besides the formation of the relevant O-upd which we cannot explain at this point. Therefore, the relevant charge of the O-upd was identified as the extra visible between 300 and 1000 mV (Fig. S1e). Additionally, we observe additional charges being reduced at potentials below 300 mV, which is magnified in Fig. S1e. If atomic oxygen is responsible for the O-upd charge, this could be the reduction of more stable oxygen species, closer to Pt-

Oxide, that need more time to be formed compared to the initial "faster" O-upd. This would also explain why some electrochemists (not published to our knowledge) observe, in some instances, that cycling into the HER region is necessary to reactivate the platinum surface. This charge could also stem from impurities, given enough time to diffuse to the electrode. Overall, this means that the potentiodynamic is preferable over the chronoamperometric method in determining the relationship between the O-upd charge and the ORR activity.

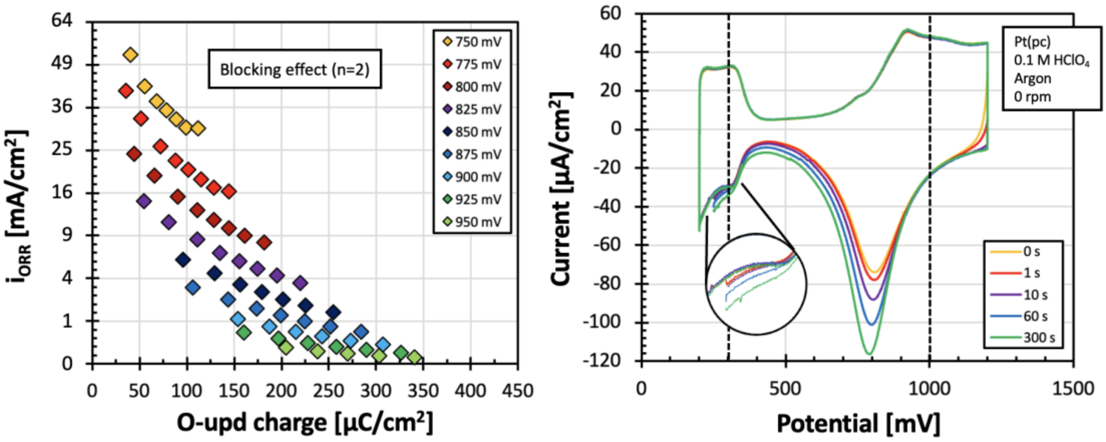

Fig. S1e| Left Blocking effect as in Fig. 3d in the main text for n=2. **Right** CVs displaying how the O-upd charge was extracted after different potential hold times at 1200 mV. The dashed lines represent the voltage limits in between the O-upd charge was determined by adding the respective charge to the charge of the 0s-curve which charge was determined by using the default method.

Extraction of the kinetic parameters for Pt(pc) in H_2SO_4 and on Pt/C

The results in sulfuric acid are very similar to that in perchloric acid, apart from the decreased exchange current density (Fig. S1f). The analysis of the cathodic branch on Pt/C in $HClO_4$ is not as clean compared to the other examples. However, it's O-upd anodic branch follows the Tafel behavior and we deem the overall analysis valid. Generally, the "shorter" the extrapolation, the cleaner is the Tafel analysis.

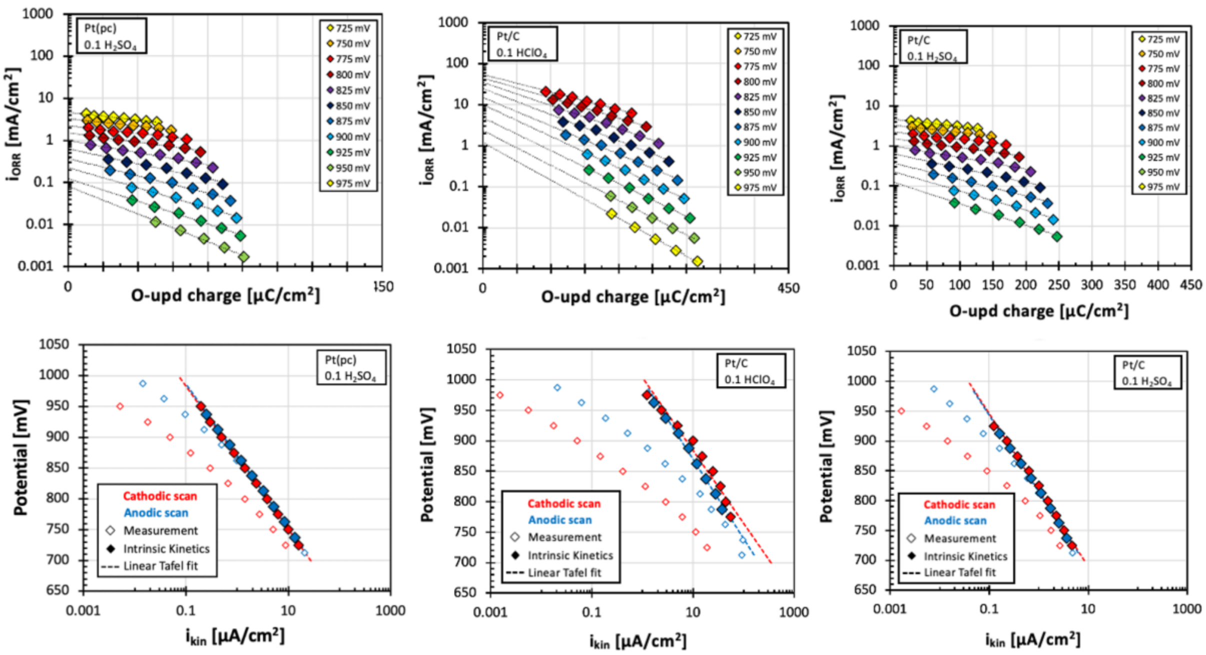

Fig. S1f| The construction of the Tafel plot as in Fig. 3e and Fig. 4a in the main text on Pt(pc) in 0.1M H_2SO_4 and Pt/C in 0.1 M $HClO_4$ and 0.1 M H_2SO_4.

Platinum alloys

The stable CV of freshly polished Pt, Pt_3Co, and Pt_3Ni are shown in Fig. S1g. When their surface is not continuously cycled above 1000 mV, surface reconstruction can be prevented due to only limited O-upd formation. This is desired for the Pt alloys, since the surface reconstruction supposedly alters the protective Pt overlayer that prevents the dissolution of the non-recoverable allowing metals. All materials show a similar CV with a depressed H-upd region. Even when cycled extensively, the H-upd features remain somewhat depressed of the alloys compared to pure Pt (not shown). Obtaining stable CVs could be greatly accelerated if the freshly polished surface was cycled for a limited number of cycles (≤50) to 1050 mV before setting 1000 mV as the permanent measurement limit.

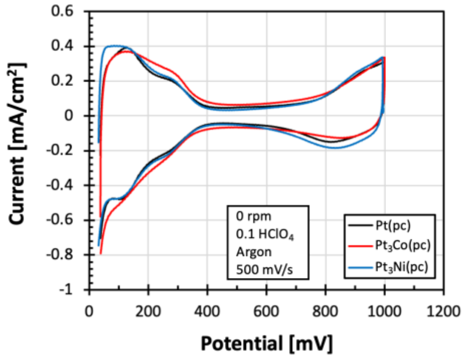

Fig. S1g| CVs of Pt3Co and Pt3Ni after polishing and cycling to a maximum of 1000 mV.

The O-upd and OER at different scan rates

Conducting the OER measurements at lower scan rates lengthen the time spend in any potential interval, increasing the amount of O-upd charge. This in turns reduces the OER currents (Fig. S1h) in agreement with the equations in the main text.

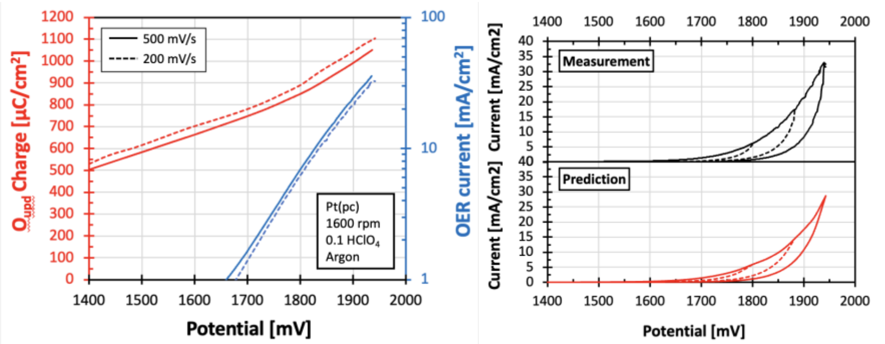

Fig. S1h| Left O-upd and currents in the OER region at different scan rates. **Right** A comparison between measurement and prediction of the OER for 200 mV/s (left).

The O-upd and OER in 0.1 M H_2SO_4 and 0.1M HCl

From Fig. S1i one finds that the OER in the presence of bisulfate is indistinguishable from the OER in $HClO_4$. In HCl chlorine is evolving until the mass transport limit of Cl^- ions is reached (not shown) and the OER is dominating.

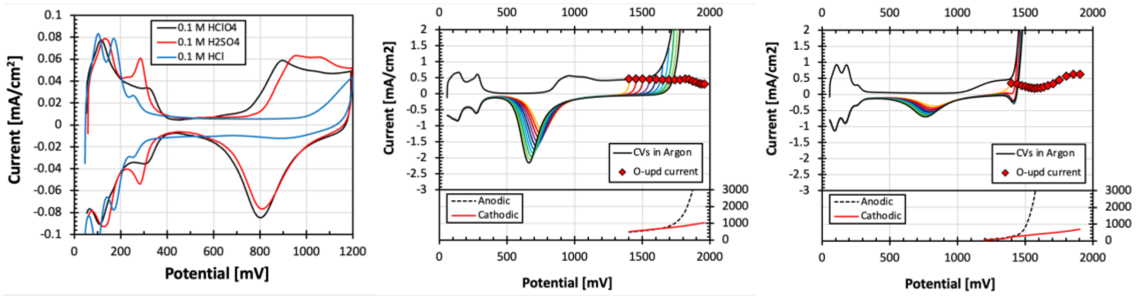

Fig. S1i| Left CVs in different electrolytes and the O-upd in specifically adsorbing electrolytes. **Center** The effect on the OER (H_2SO_4). **Right** Chloride evolution (HCl)

Raw data and processed results

To process the relatively large amount of acquired data, a semi-automized java tool was developed utilizing drag 'n' drop of EC-lab text files (.mpt), performing fully customizable data smoothing, HFR correction, RHE correction, background correction, CO displacement charge extraction, H-upd charge extraction and the Koutecký-Levich analysis. Without this tool, this study would not have been possible. The output files are in a .csv or .xlsx file format, including both the raw and processed data sets. This tool can be made available upon request.

2. Results of the computational method and processing

The change in binding energy of ORR intermediates O by the presence of *O on Pt(111) and Pt(100) is calculated as follows from Boltzmann weighted samplings of *O configurations and sites for the ORR intermediates:

$$\Delta_Q \Delta U_{f,i}(Q) = \Delta U_{f,i}(Q) - \Delta U_{f,i}(Q=0) \tag{S2a}$$

$$\Delta U_{f,i}(Q) = U_i(Q) - U_{\text{empty}}(Q) + U_{i,\text{Other}}(Q) \tag{S2b}$$

$$\frac{\partial U_{i,\text{Other}}(Q)}{\partial Q} = 0 \tag{S2c}$$

$$\Rightarrow \Delta_Q \Delta U_{f,i}(Q) = U_i(Q) - U_i(Q=0) - \left(U_{\text{empty}}(Q) - U_{\text{empty}}(Q=0)\right) \tag{S2d}$$

Boltzmann-weighing was performed using the following mathematical expressions:

i = Intermediate iterator, j = Site iterator,

k = O-configuration iterator, l = coverage iterator

$$w_{k,l} = \frac{\exp\left(-\frac{U_{0,0,k,l}}{RT}\right)}{\sum_k \exp\left(-\frac{U_{0,0,k,l}}{RT}\right)} \tag{S2e}$$

$$w_{\mathrm{i,j,k,l}} = \frac{\exp\left(-\frac{U_{\mathrm{i,j,k,l}}}{RT}\right)}{\sum_j \exp\left(-\frac{U_{\mathrm{i,j,k,l}}}{RT}\right)} \tag{S2f}$$

$$U_{i,k,l} = \sum\nolimits_j w_{\mathrm{i,j,k,l}} \cdot U_{i,j,k,l} \tag{S2g}$$

$$U_{i,l} = \sum\nolimits_k w_{\mathrm{k,l}} \cdot U_{i,k,l} \tag{S2h}$$

$$U_i(Q) = U_{i,l} \tag{S2i}$$

***O_{upd} and ORR intermediate structures**

In Fig. S2a-g the values $U_{\mathrm{i,j,k,l}}$ for the different ORR intermediates and *O_{upd} structures can be found. These were used to calculate $U_i(Q)$ that is then used to calculate $\Delta_Q \Delta U_{f,i}(Q)$ which is displayed in Fig. 8a in the main text.

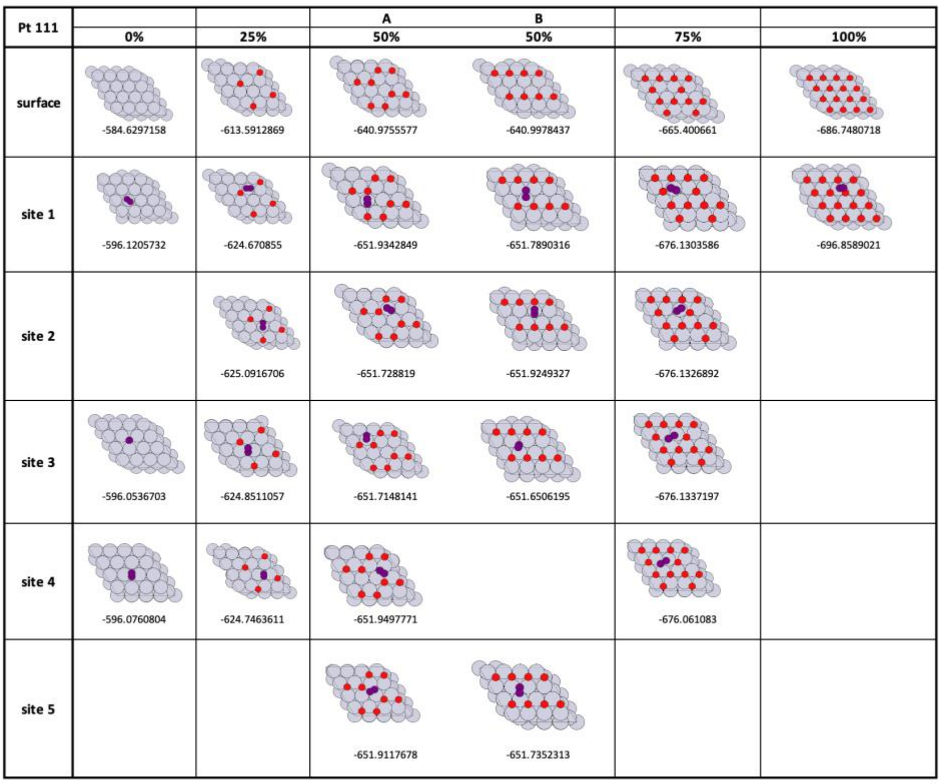

Fig. S2a| Energies of *OO intermediates on various *O_{upd} adsorption structures on Pt(111).

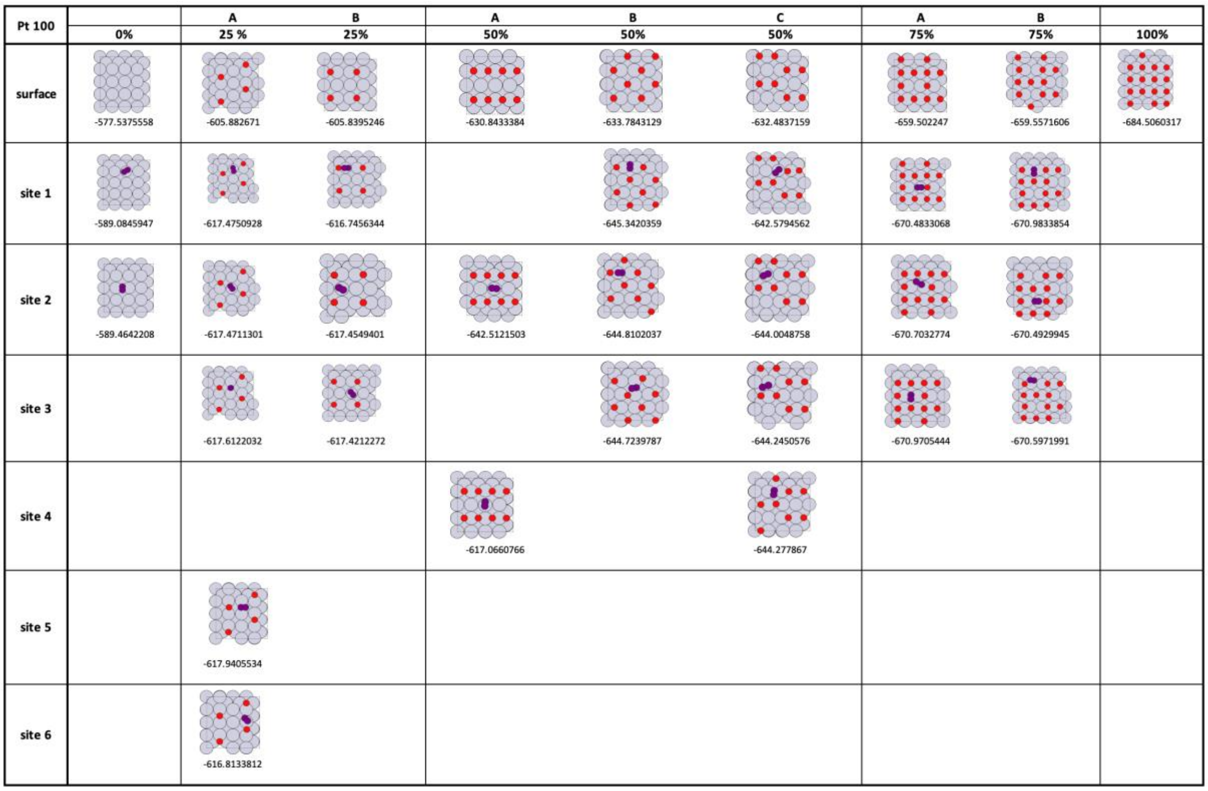

Pt 100	0%	A 25 %	B 25%	A 50%	B 50%	C 50%	A 75%	B 75%	100%
surface	-577.5375558	-605.882671	-605.8395246	-630.8433384	-633.7843129	-632.4837159	-659.502247	-659.5571606	-684.5060317
site 1	-589.0845947	-617.4750928	-616.7456344		-645.3420359	-642.5794562	-670.4833068	-670.9833854	
site 2	-589.4642208	-617.4711301	-617.4549401	-642.5121503	-644.8102037	-644.0048758	-670.7032774	-670.4929945	
site 3		-617.6122032	-617.4212272		-644.7239787	-644.2450576	-670.9705444	-670.5971991	
site 4				-617.0660766		-644.277867			
site 5		-617.9405534							
site 6		-616.8133812							

Fig. S2b| Energies of *OO intermediates on various *O_{upd} adsorption structures on Pt(100).

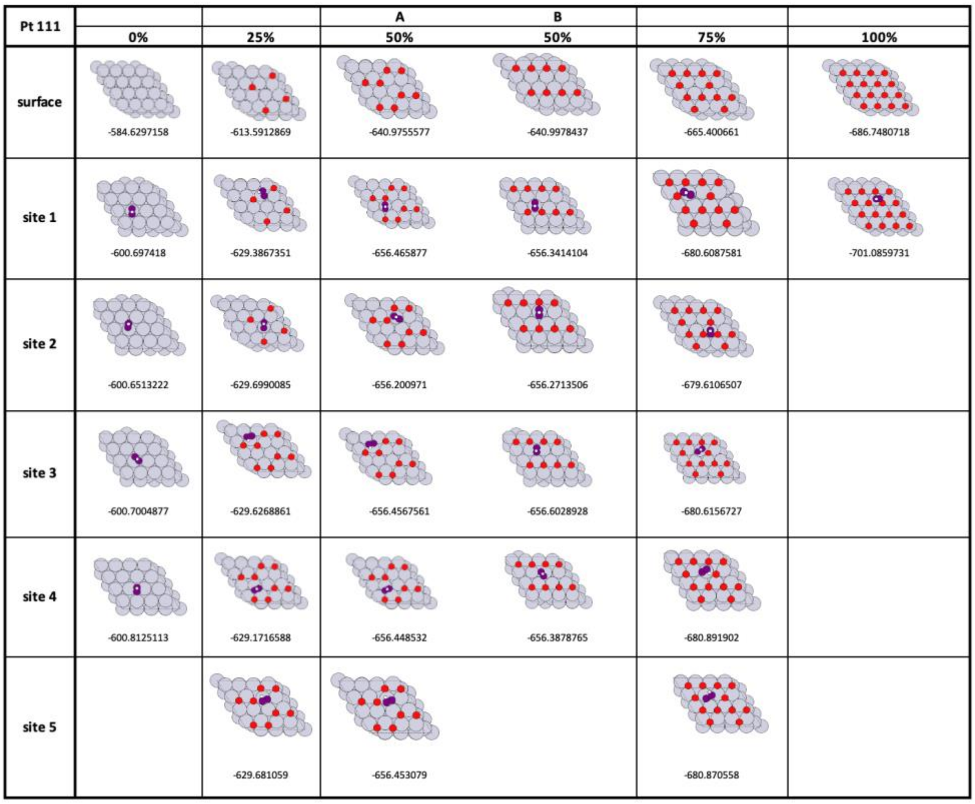

Pt 111	0%	25%	A 50%	B 50%	75%	100%
surface	-584.6297158	-613.5912869	-640.9755577	-640.9978437	-665.400661	-686.7480718
site 1	-600.697418	-629.3867351	-656.465877	-656.3414104	-680.6087581	-701.0859731
site 2	-600.6513222	-629.6990085	-656.200971	-656.2713506	-679.6106507	
site 3	-600.7004877	-629.6268861	-656.4567561	-656.6028928	-680.6156727	
site 4	-600.8125113	-629.1716588	-656.448532	-656.3878765	-680.891902	
site 5		-629.681059	-656.453079		-680.870558	

Fig. S2c| Energies of *OOH intermediates on various *O_{upd} adsorption structures on Pt(111).

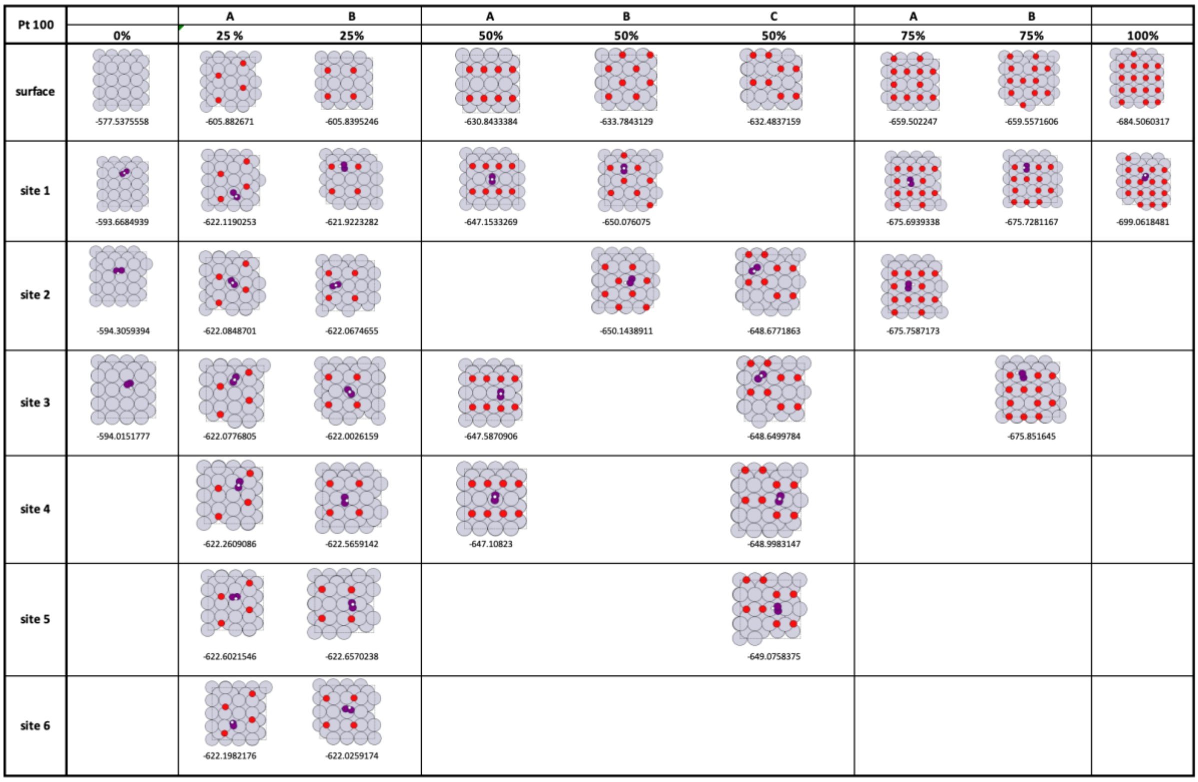

Pt 100	0%	A 25 %	B 25%	A 50%	B 50%	C 50%	A 75%	B 75%	100%
surface	-577.5375558	-605.882671	-605.8395246	-630.8433384	-633.7843129	-632.4837159	-659.502247	-659.5571606	-684.5060317
site 1	-593.6684939	-622.1190253	-621.9223282	-647.1533269	-650.076075		-675.6939338	-675.7281167	-699.0618481
site 2	-594.3059394	-622.0848701	-622.0674655		-650.1438911	-648.6771863	-675.7587173		
site 3	-594.0151777	-622.0776805	-622.0026159	-647.5870906		-648.6499784		-675.851645	
site 4		-622.2609086	-622.5659142	-647.10823		-648.9983147			
site 5		-622.6021546	-622.6570238			-649.0758375			
site 6		-622.1982176	-622.0259174						

Fig. S2d| Energies of *OOH intermediates on various *O_{upd} adsorption structures on Pt(100).

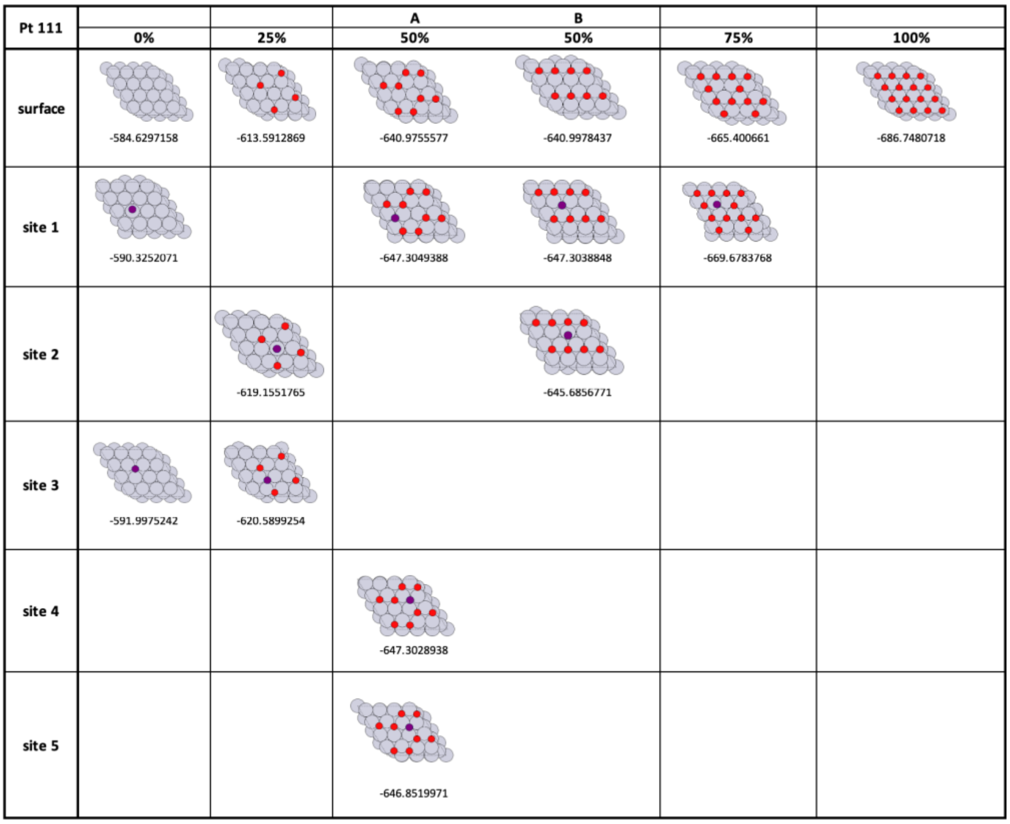

Pt 111	0%	25%	A 50%	B 50%	75%	100%
surface	-584.6297158	-613.5912869	-640.9755577	-640.9978437	-665.400661	-686.7480718
site 1	-590.3252071		-647.3049388	-647.3038848	-669.6783768	
site 2		-619.1551765		-645.6856771		
site 3	-591.9975242	-620.5899254				
site 4			-647.3028938			
site 5			-646.8519971			

Fig. S2e| Energies of *O intermediates on various *O_{upd} adsorption structures on Pt(111).

Pt 100		A	B	A	B	C	A	B	
	0%	25 %	25%	50%	50%	50%	75%	75%	100%
surface	-577.5375558	-605.882671	-605.8395246	-630.8433384	-633.7843129	-632.4837159	-659.502247	-659.5571606	-684.5060317
site 1	-583.3543672	-611.6846575	-611.2474634	-	-640.2524466		-665.8138007	-665.8364507	
site 2	-584.7287191	-611.6907919	-611.6468161	-636.6442002		-638.137415			
site 3		-613.0973274							
site 4		-612.5087098	-612.1605163			-639.2920388			
site 5		-613.0957017	-612.9438752						
site 6		-612.1841079							

Fig. S2f| Energies of *O intermediates on various *O_{upd} adsorption structures on Pt(100).

Pt 111			A	B		
	0%	25%	50%	50%	75%	100%
surface	-584.6297158	-613.5912869	-640.9755577	-640.9978437	-665.400661	-686.7480718
site 1	-595.7229498	-624.2031844	-651.6460206	-651.3566829	-675.7255564	-695.4843689
site 2	-596.0312154	-624.6632296	-651.2923422		-675.7299965	
site 3			-651.2430467		-675.7485686	
site 4	-596.0441498	-624.7044547	-651.6935541	-651.4951316	-675.7497528	
site 5				-651.5316112		

Fig. S2g| Energies of *OH intermediates on various *O_{upd} adsorption structures on Pt(111).

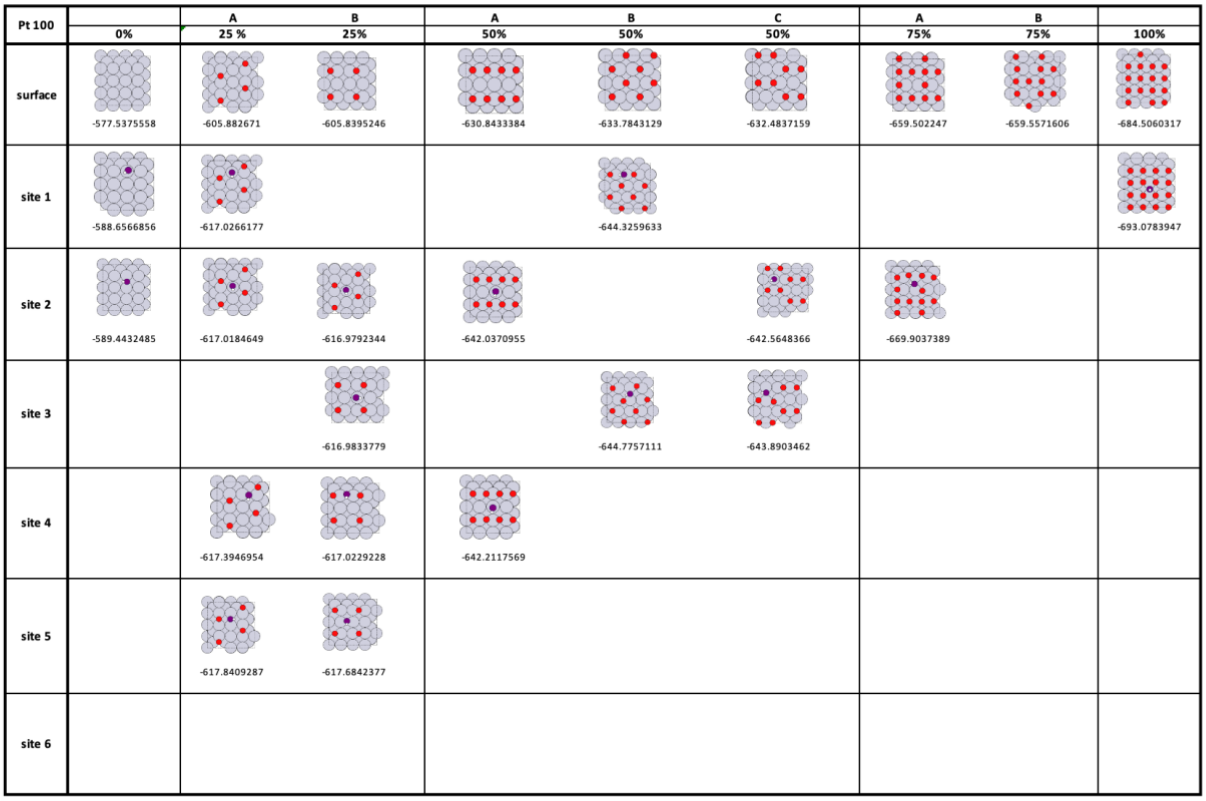

Fig. S2f| Energies of *OH intermediates on various *O_{upd} adsorption structures on Pt(100).

3. X-ray Photoemission spectroscopy (XPS)

On the decrease of adventitious O: When a freshly polished or long stored Pt electrode is submerged in the electrolyte and the initial scan is performed from the open circuit voltage in the cathodic scan direction into the H-upd region one typically observes a large reduction peak. This correlates with a large amount of adventitious oxygen removed from the Pt surface compared to an electrochemical measured Pt electrode (Fig. 5d and Fig. S3a). In the survey spectra we found the expected elements of oxygen, platinum, and the respective alloy element. When the sample was polished right before XPS, we found minor traces of sodium and nitrogen (Fig. 4b).

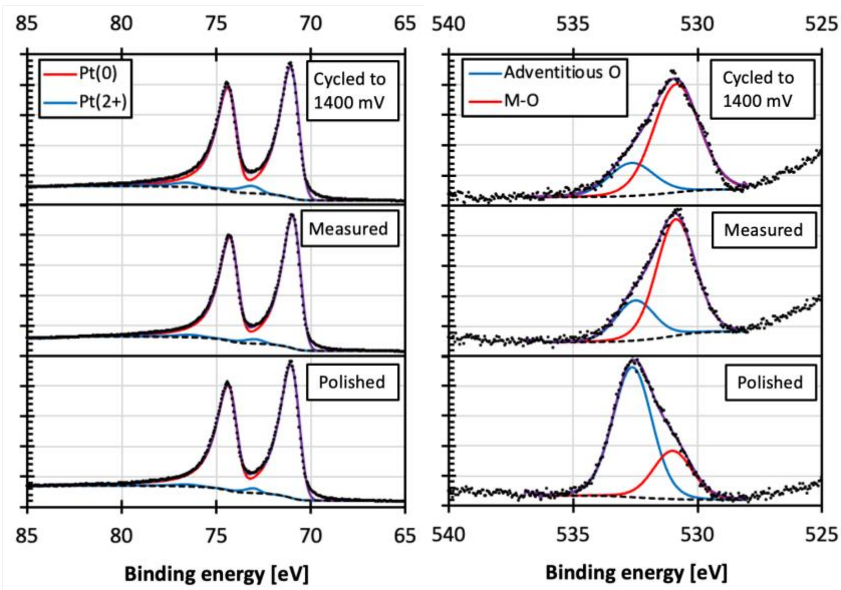

Fig. S3a| XPS spectra of the platinum Pt 4f and Oxygen O 1s peak.

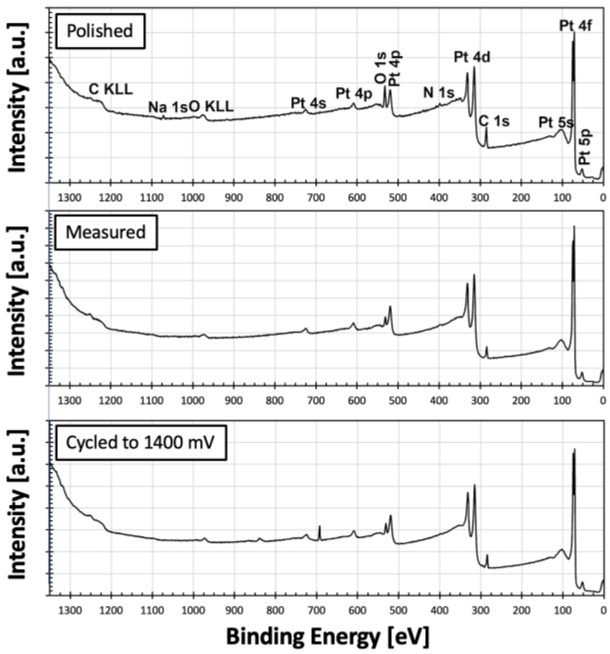

Fig. S3b| XPS surveys on the platinum surfaces.

4 Powder X-ray diffraction (XRD)

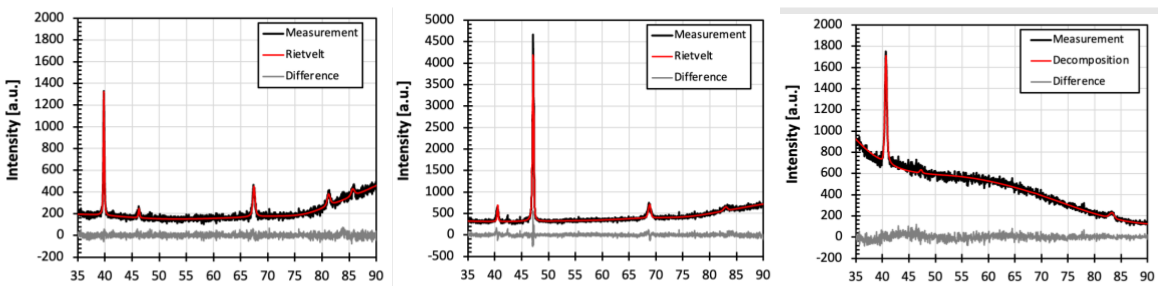

Fig. 4a| XRD spectrum of the Pt (left), Pt_3Co (center), and Pt_3Ni (right) crystal.

From Rietveld refinement of the XRD spectra we find that the lattice constant of the Pt, Pt_3Co, and Pt_3Ni crystal is 3.9303 nm, 3.8615 nm, and 3.8489 nm, respectively.